Article:
Yang, Y., Aydin, A., Mumtaz, K. et al. (2026) New insights on the influence of hard transformed regions created on R260 rails using lasers on damage behaviour during rolling-sliding contact tests. Wear, 591. 206615. ISSN: 0043-1648

https://doi.org/10.1016/j.wear.2026.206615

NEW INSIGHTS ON THE INFLUENCE OF HARD TRANSFORMED REGIONS CREATED ON R260 RAILS USING LASERS ON DAMAGE BEHAVIOUR DURING ROLLING-SLIDING CONTACT TESTS

Y. Yang [a], A. Aydin [a], K. Mumtaz [a], A. Meierhofer [b], R. Lewis [a*]

[a] School of Mechanical, Aerospace and Civil Engineering, University of Sheffield, Mappin Street, Sheffield S1 3JD, UK
[b] Virtual Vehicle Research Gmbh, Inffeldgasse 21/A/I, 8010 Graz, Austria

[*] E-mail: roger.lewis@sheffield.ac.uk

Abstract: This research examines the influence of laser-induced hard transformed regions (consisting of white and likely brown etching layers) on the damage behaviour of R260 rail steel under rolling–sliding contact conditions. The laser-based approach was found to produce very consistent transformed regions across different specimens. The research explores how the transformed regions contribute to crack initiation and propagation, particularly at the interface with the substrate material and within the transformed region itself. Crack formation was consistent in terms of location, angle, and length for regions of the same geometry, while systematic variations in crack position and length were observed when comparing regions of different lengths. Localised material deformation, including unique material flow patterns at the trailing edge, was found to play a key role in crack development. The findings provide deeper insight into rail surface degradation mechanisms and have implications for the design, treatment, and maintenance of railway components. The consistency of the layer-based approach and the possibility to efficiently test many hard transformed regions for the first time has allowed generation of repeatable and consistent data sets that can be used with confidence as inputs for rail damage modelling and for providing a benchmark for comparing against other rail grades.

Keywords: Rail-wheel tribology; White Etching Layer; hard transformed regions; Crack propagation; Laser processing

1. Introduction

The development of rail surface defects, particularly squats, remains a significant concern in the realm of railway engineering. Squat defects typically arise due to wheel-rail rolling contact fatigue (RCF) and are closely associated with the formation of phase-transformed regions consisting of brown etching layers (BEL) and white etching layers (WEL) on both wheels and rails [1]. These layers are characterized by their high hardness and distinct microstructural properties, resulting from localized high temperatures and pressures during wheel sliding [2]. Their formation is often linked to severe contact conditions, such as wheel slips, braking, or traction forces, which produce localised thermal and mechanical transformations at the rail surface which may induce further failures during subsequent wheel passages [3].

Although BELs and WELs are very common in the existing railway systems, there is still a lack of systematic understanding regarding their mechanical behaviour and influence on fatigue damage under the rolling-sliding conditions. WELs showed a critical role in accelerating surface-initiated fatigue damage, including crack initiation, propagation, and ultimately rail surface failure [4], [5]. The presence of WEL can reduce the fatigue life of rails and compromise operational safety, particularly in high-traffic or high-traction areas such as curves, switches, and braking zones [6], [7]. Despite being a frequent topic of research, however, variability in field conditions has made it difficult to isolate and study the precise mechanisms of crack development at and around WEL regions. Understanding the behaviour of WELs under controlled laboratory conditions is essential for linking microstructural characteristics to observed surface degradation and for developing predictive maintenance strategies.

Several approaches have been employed in previous research to generate WELs for experimental analysis. These include using a spot welder and conducted fully sliding tests using a twin-disc rig [3], applying arc welding to small scale specimens [6] and generation using pin-on-disc tests [8]. More recently, laser surface treatments have gained traction due to their precision, repeatability, and ability to localise the thermal input by enabling controlled creation of WELs with desired dimensions and morphologies [9], [10]. Laser processing allows for high spatial resolution, minimal distortion to the surrounding material, and the possibility of tailoring

layer properties through variation in scanning parameters such as power, speed, and spot size [9], [10], [11], [12].

However, there remains debate over whether laser-induced WELs accurately replicate the complex and often heterogeneous microstructures of in-service WELs formed under dynamic wheel-rail interaction. Differences in residual stress states, hardness gradients, and phase composition have been reported between laser-induced and naturally formed WELs, which could influence their mechanical performance and the way cracks initiate and propagate through these regions [13], [14], [15]. Thus, while lasers provide a controllable platform for studying WEL formation and its effects, it is essential to validate whether these artificial WELs behave similarly to their in-service counterparts under representative loading conditions. Testing of WELs created on twin specimens manufactured from wheel steels has been carried out [12], [13], while different rail materials with thicker WEL have been reported in previous studies [16], [17] however, more uniformed and thinner WEL have not yet been studied.

Understanding how WELs form and behave is becoming increasingly important as modern railway systems face higher axle loads, sharper curves, and more frequent acceleration and braking. These operating conditions accelerate the formation of WELs and related surface damage, making regular track inspection, grinding, and replacement even more critical [16]. Gaining deeper insights into how WELs contribute to damage mechanisms can help inform predictive modelling, enhance surface treatment methods, and guide more effective maintenance strategies.

This study seeks to contribute to this understanding by investigating the influence of laser-induced hard transformed regions on R260 rail steel under twin-disc rolling-sliding contact tests. A key aim is to determine how consistently such laser-generated transformed regions reproduce crack behaviour, particularly in terms of initiation and propagation patterns. Special attention is given to crack development at the interface with the substrate and within the transformed region itself. R260 rail and ER8 wheel materials were selected to represent common wheel-rail material pairings used in Europe and elsewhere.

An important improvement in this study is the ability to consistently create transformed regions through laser processing, with high repeatability in crack location, orientation, and depth during rolling-sliding contact testing. This controlled approach allows for more reliable analysis of damage mechanisms and offers a solid foundation for future research into surface-initiated fatigue. Ultimately, the goal is to evaluate the utility of laser-induced transformed regions as reliable analogues for in-service transformed regions and to better understand how these microstructural features contribute to crack development and rail surface degradation.

2. Methodology

In this study, R260 grade rail material and ER8 grade wheel material were selected to conduct the tests. Their chemical compositions are presented in Table 1. The specimens were extracted from the contact interface region of the rail head and the wheel, as can been seen in Figure 1, while the subsequent rolling/sliding loading conditions are representative of service contact, the initial microstructure prior to laser treatment remains undeformed. Table 2 summarises the laser treatment parameters used to generate the WEL was carried out using a diode laser system operating at full power of 42 Watts. The laser was scanned across the rail disc surface at a constant speed of 4.0 mm/s, with a hatch spacing of 100 μm between adjacent scan tracks. To enhance laser energy absorption and ensure repeatable thermal input, the rail surface was treated under air-quenched during processing. A single serpentine scanning strategy was employed, followed by one repeat scan that retraced the same path as the previous pass. This scanning approach ensured a uniform thermal exposure along the treated region while maintaining a controlled and reproducible transformed region thickness across all specimens. The selection of the laser parameters has been detailed in previous work [9]. The laser treatment process was conducted using a customised set-up as shown in Figure 2, which enabled the creation of nine distinct transformed regions formations (3 repeats of 3 different target transformed region lengths of 600, 900 and 1200 μm) on three R260 rail disc samples as shown in Table 3 with same targeted thickness of 60 μm. This thickness falls within the range commonly reported for in-service WELs on straight-track pearlitic rails, where crack initiation and delamination are frequently observed [18], [19], [20]. Thicker layers are typically associated with more severe conditions such as tight curves or wheel materials and were therefore not considered in this study.

Table 1 *Chemical composition (wt%) of rail and wheel specimens used in this research.*

Chemical Composition	**C**	**Si**	**Mn**	**P**	**S**	**Cr**	**V**	**Cu**	**Ti**	**Ni**	**Mo**	**Al**
Rail - R260	0.736	0.27	1.056	0.032	0.023	0.026	0.003	0.002	0.016	0.021	0.006	-
Wheel - ER8	0.542	0.253	0.734	0.011	0.06	0.141	0.006	0.065	0.002	0.12	0.048	0.027

Table 2 *Laser parameters used in generate transformed samples.*

Parameter	**Setting**
Laser type	Diode
Laser power (Watts)	42
Scan speed (mm/s)	4.0
Hatch spacing (μm)	100
Scanning strategy	Single serpentine + one repeat scan
Cooling condition	Air quenching
Target WEL thickness (μm)	60

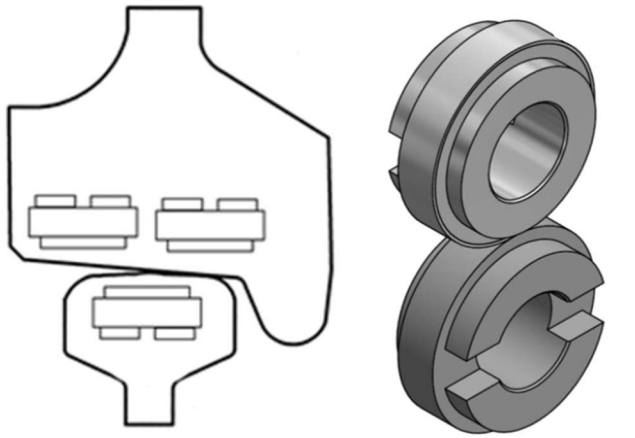

Figure 1 *(a) Schematics of disc extraction location from wheel and rail; (b) Wheel and rail disc set-up in the twin disc machine.*

While just using thermal processing will mean that the transformed region may not be exactly representative of that produced using the thermo-mechanical loading during a wheel slide or during grinding. If a hard layer can be achieved of the similar dimensions and hardness to a field WEL it can still provide a useful tool for testing to understand transformed region influence on crack formation during subsequent wheel passes [20]. The laser processed samples were subsequently tested in a twin disc rig under rolling–sliding conditions as illustrated in Figure 3, with the wheel material (ER8 grade) interacting with the treated rail discs. The test conditions were as follows to replicate realistic operational stresses encountered in service: a contact pressure of 1500 MPa, a rotational speed of 400 rpm, and a test sequence consisting of 4,000 cycles with 1% slip to introduce the crack initiation and then followed with 10,000 cycles with 0% slip to grow the cracks. The numbers of cycles and slippages were selected based on laboratory-based twin-disc test trials to avoid the transformed region being removed too quickly.

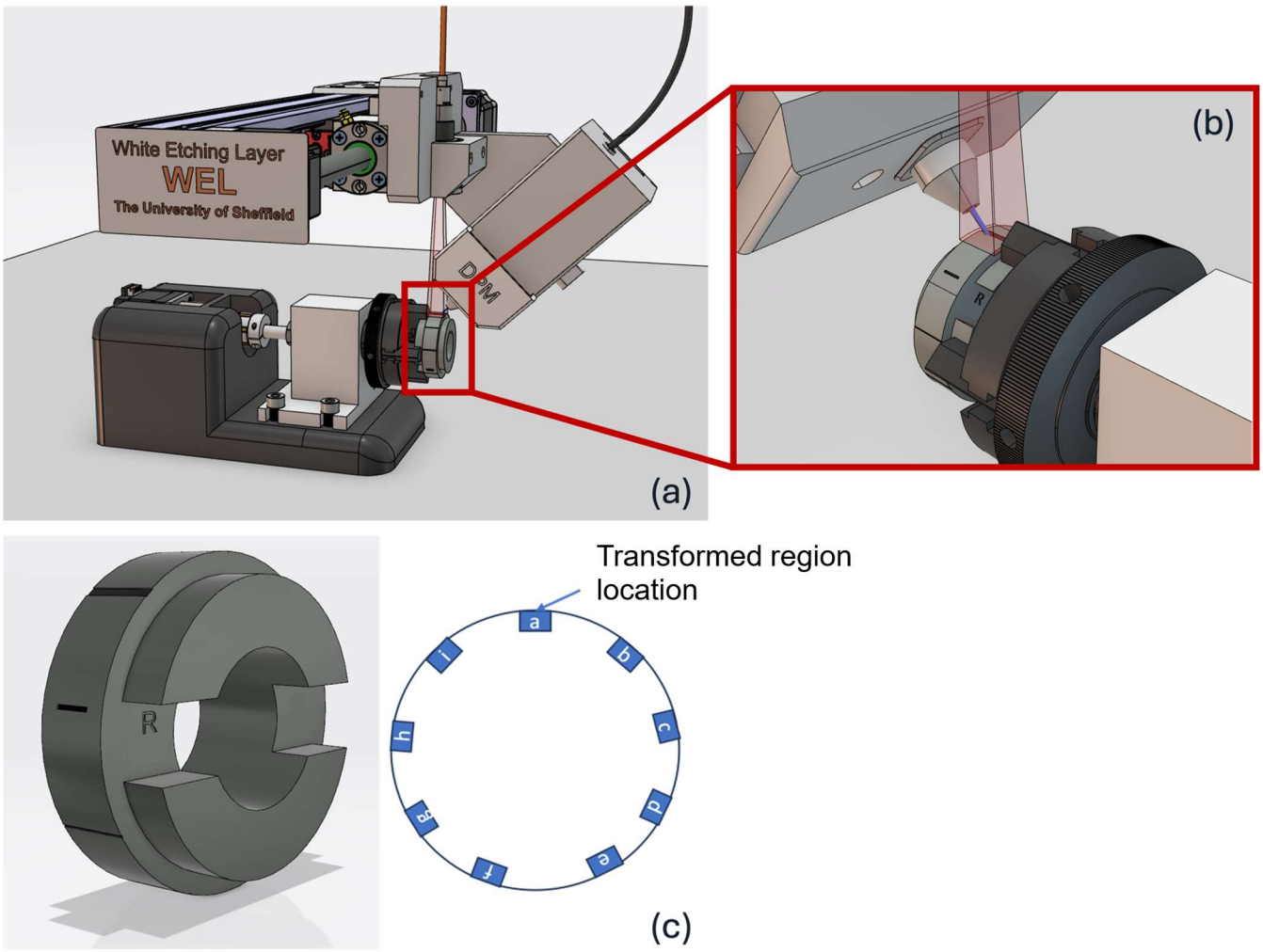

Figure 2 *(a) Laser-based transformed region creation set-up; (b) Zoom-in view of laser treatment on rail disc; (c) 9 locations of transformed regions on rail disc.*

Table 3 *Transformed region parameters against locations.*

Disc	Target Transformed Region Length (µm)	Target Region Thickness (µm)	Region Location
R260	600	60	A, D, G
	900	60	B, F, H
	1800	60	C, E, I

Post-testing, the surface and microstructure of the laser-treated rail specimens were analysed using optical microscopy, scanning electron microscopy (SEM), and micro-hardness measurements. The microstructural analysis focused on crack formation at the transformed region/substrate interface, including both leading and trailing edge cracks, as well as internal cracks within the transformed region itself. Additionally, hardness maps were generated to provide further insight into material deformation patterns around the transformed region. The relationship between material deformation and crack growth was examined by correlating the hardness distribution with observed crack locations.

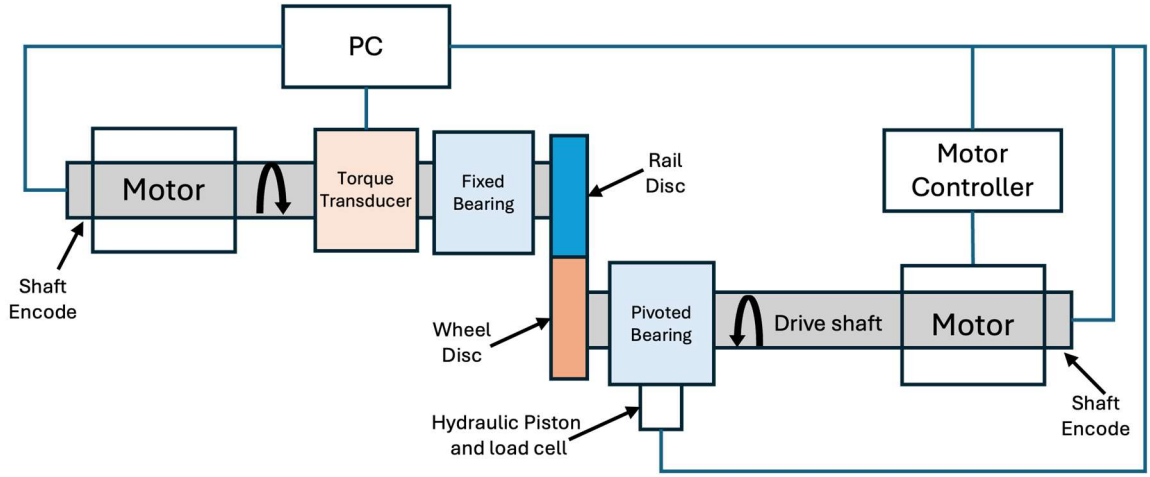

Figure 3 *Schematic of twin disc test set-up.*

3. Results

3.1. WEL Geometry formation

Using a customised laser-based set-up for the transformed region generation, three R260 rail discs were prepared, each containing nine designated transformed region locations. Examples of 3 different lengths of transformed region are shown in Figure 4(a-c), while the original microstructure of R260 has been shown in Figure4(d). The actual average lengths of the transformed regions across the three discs are shown in Figure 4(e), which demonstrates a high degree of consistency and control, with average transformed region length values of 618 µm, 897 µm, and 1782 µm, respectively.

Detailed microstructural examination of the laser-treated areas referred to here as transformed regions, confirmed that these regions were not composed of a uniform white etching layer (WEL) alone. Instead, they consisted of a combination of a near-surface WEL and what is likely a brown etching layer (BEL) or tempered region, with local variations in phase constitution across the transformed depth. Despite this microstructural heterogeneity, the different parts of the transformed region exhibit significantly higher hardness than the bulk pearlitic microstructure. As a result, from a mechanical perspective, the wheel-rail contact experiences these regions as discrete hard patches of material with well-defined geometric dimensions.

The transformed region thickness was found to be consistent across all samples, with an average value of approximately 62 µm, as presented in Figure 5. Furthermore, as shown in Figure 6, the transformed region thickness appears to be independent of transformed region length, as no significant correlation was observed when comparing the average values across the three discs.

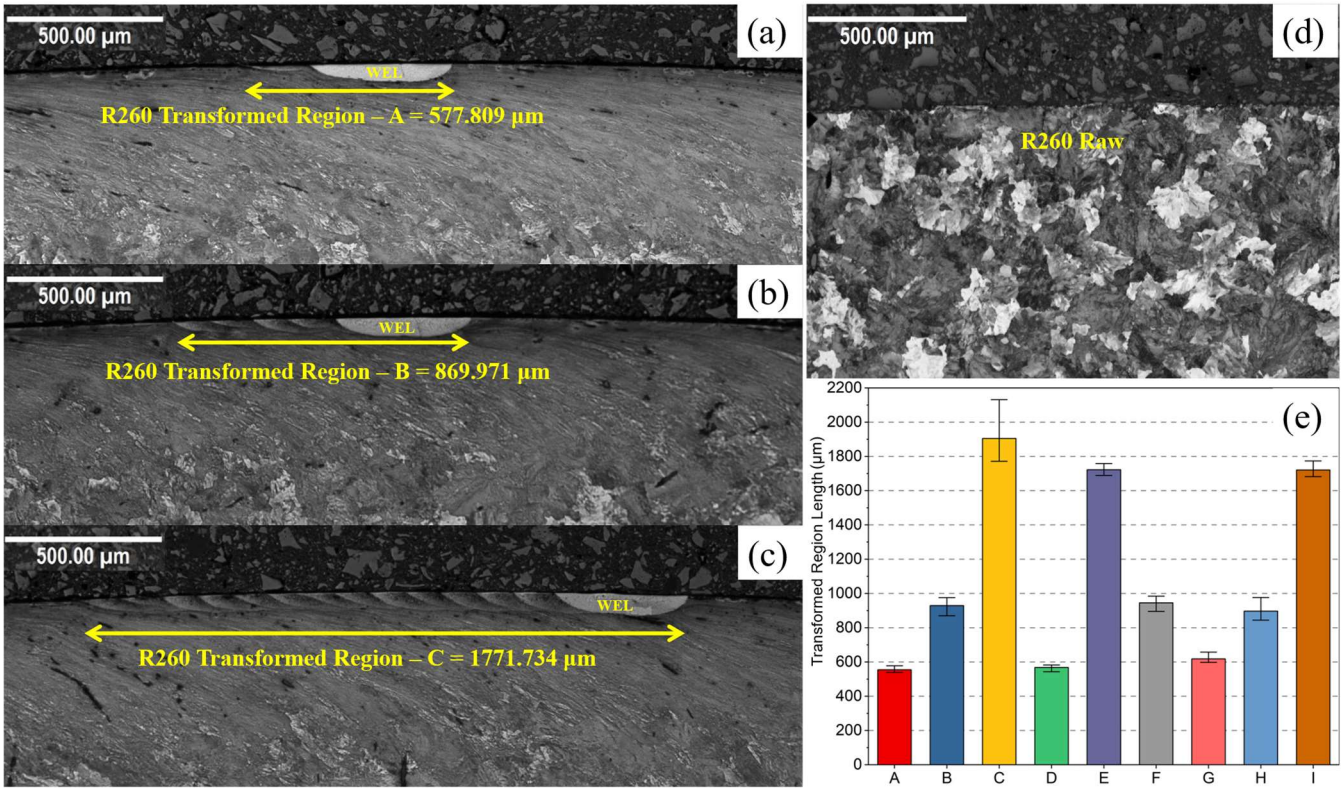

Figure 4 *(a-c) Samples of different lengths of transformed region; (c) Microstructure of R260 rail material; (d) Bulk R260 microstructure; (e) Average transformed region length for 9 locations averaged across 3 discs with "error bars" showing the standard deviation.*

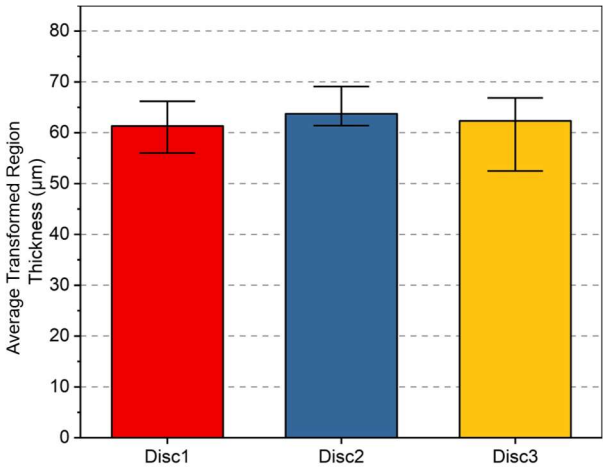

Figure 5 *Average transformed region thickness for Disc 1, 2 and 3.*

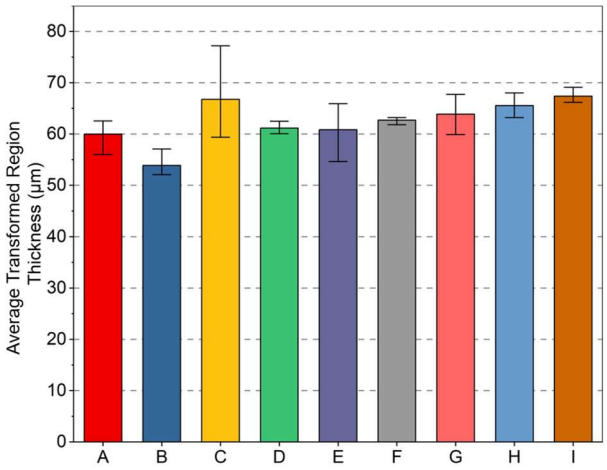

Figure 6 *Average transformed region thickness for 9 locations averaged across 3 discs.*

3.2. Crack Formation and Propagation

After twin-disc testing, three main types of cracks were observed around the transformed region. These included shallow cracks near the leading edge, deeper interface cracks near the trailing edge, and internal cracks within the WEL material. Figure 7 provides representative microstructural images of these cracks, and the leading edge crack angle and trailing edge crack angle were defined as the acute angle from the contact surface to the crack. Additionally, transformed region samples exhibited "Y-shaped" junctions at the trailing edge as the yellow curves indicated at the bottom right corner of the transformed region. These features suggest that both surface compressive forces and subsurface material flow contribute to deformation, and crack bifurcation and propagation.

The leading-edge cracks, shown in Figure 8, propagated at relatively shallow angles averaging just over 10°. These cracks curved around plastically deformed material located ahead of the WEL and did not exhibit any strong dependence on transformed region length.

At the other end, the cracks angle near the trailing edge illustrated in Figure 9 were steeper with average angles exceeding 55°. These cracks tended to follow the WEL/substrate interface. As can be seen in Figure 10(d), the length of crack propagation along the interface increased with WEL length, indicating that longer WELs may promote more extensive interfacial crack growth. Additional examples from locations A, B, and C in Figures 10(a–c) further support this observation. Moreover, as the WEL length increased, the internal crack length decreased, and the internal crack initiation point progressively shifted further away from the trailing edge.

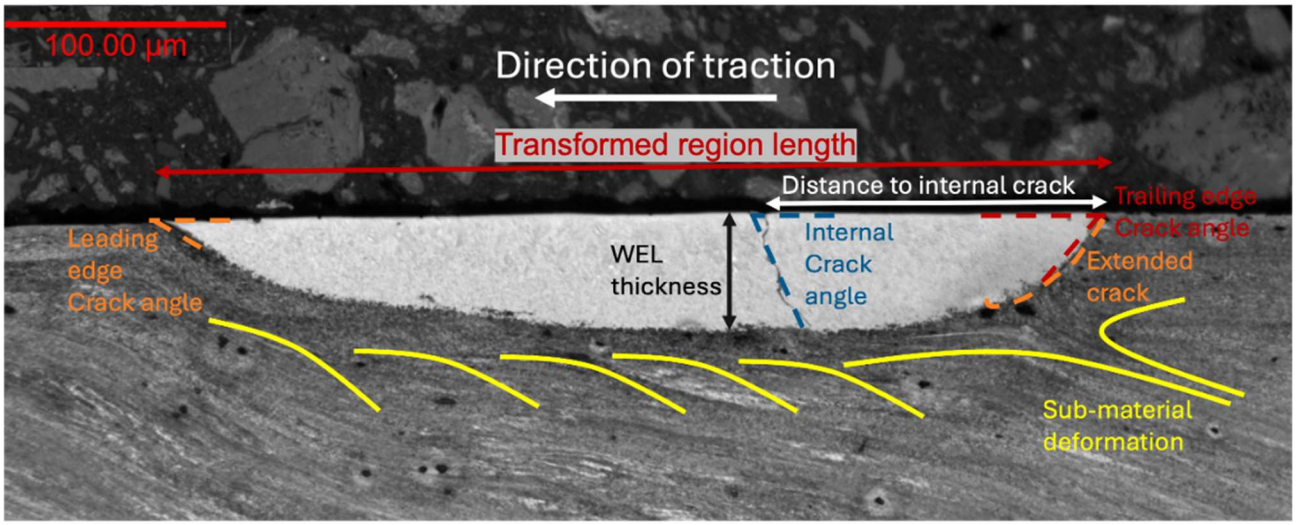

Figure 7 *Microstructure of cracks around the transformed region on a R260 grade rail surface under optical microscope.*

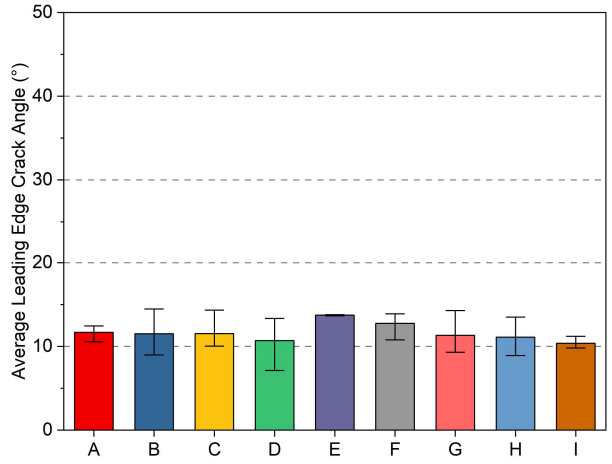

Figure 8 *Average crack angle at leading edge after twin disc test.*

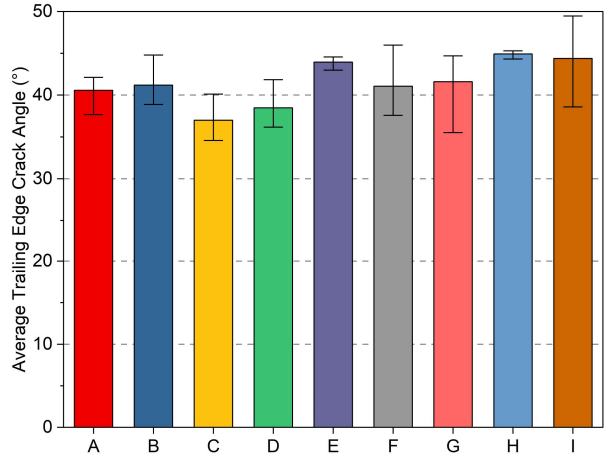

Figure 9 *Average crack angle at trailing edge after twin disc test.*

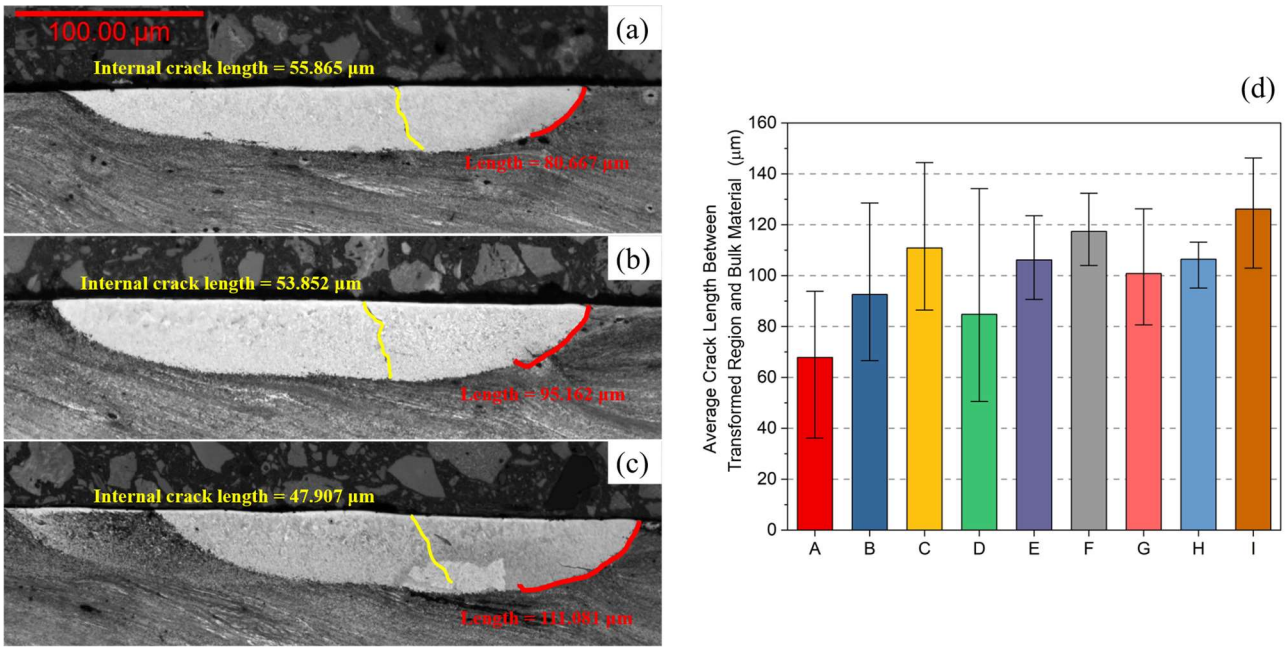

Figure 10 *(a-c) Samples of crack between transformed region and bulk material; (d) Average crack length between transformed region and bulk material.*

3.3. Crack Characteristics

The following analysis therefore distinguishes between repeatability within a given transformed region geometry and systematic trends observed across different region lengths. Internal cracking within the transformed region was a consistent feature after rolling–sliding testing. Figures 11–13 show that these internal cracks extended predominantly vertically through the transformed region material, with average lengths ranging from 38 μm to 51 μm. Shorter patches exhibited slightly longer internal cracks. The crack angles were consistently measured between 75° and 85°, and no strong correlation was found between patch length and either internal crack length or crack angle.

However, the location of internal crack initiation was found to vary with transformed region geometry. As shown in Figure 14, the distance between the trailing edge and the crack initiation point increased with increasing patch length. This indicates that while crack size and orientation remained consistent, the crack location was influenced by the longitudinal extent of the transformed region. It should be noted that these variations in crack location occur between patches of different lengths. For patches of the same length, the crack characteristics were highly repeatable in terms of location, orientation, and size.

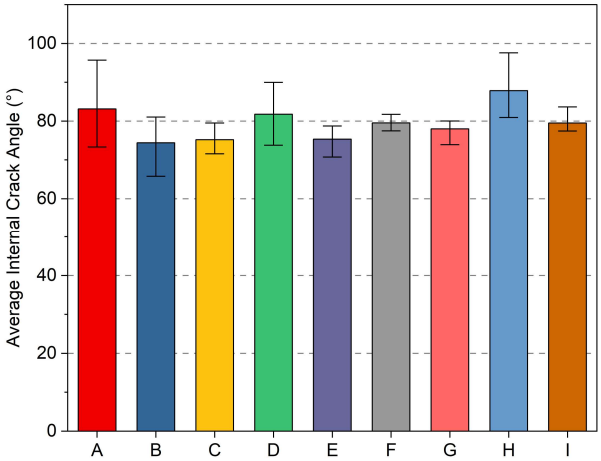

Figure 11 *Average internal crack angle across 3 discs.*

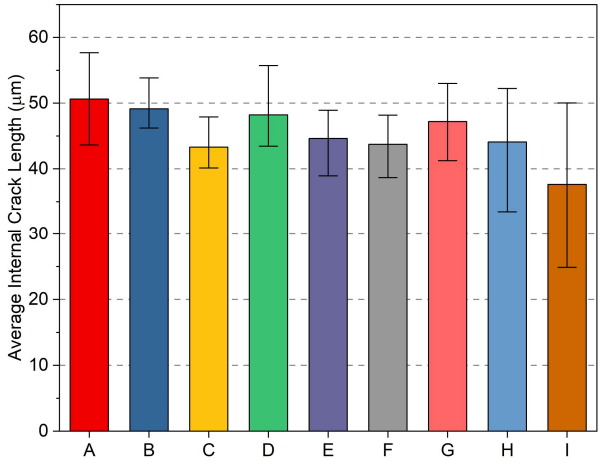

Figure 12 *Average internal crack length across 3 discs.*

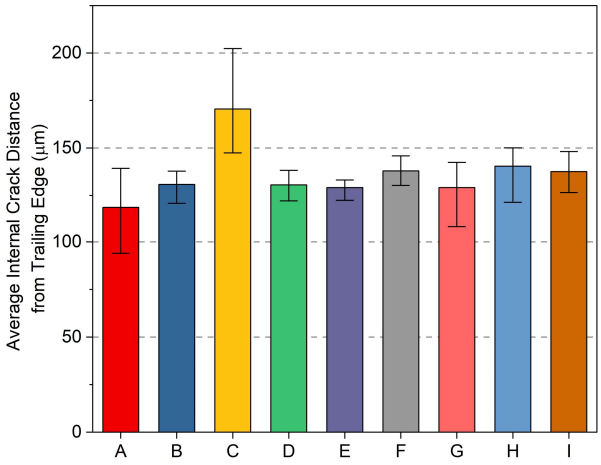

Figure 13 *Average internal crack distance from trailing edge across 3 discs.*

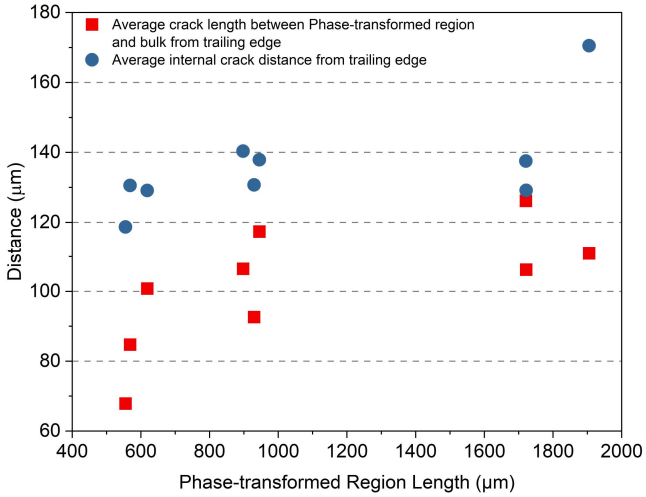

Figure 14 *Average cracks length between transformed region and bulk from the trailing edge and average internal crack distance from the trailing edge versus transformed region length across 3 discs.*

4. Discussion

4.1. Comparison with field WEL behaviour

In order to assess the validity of using laser-processed transformed regions as laboratory analogues of those formed in service, both microstructural and mechanical comparisons were undertaken. Figure 15 compares two field samples [19], [17] to a laser-generated transformed region [16]. The crack between the field WEL/BEL region can be observed from Figure 15 (a-b), while in Figure (c-d), field and laser samples can be seen to have similar length and thickness. The cracks formed are also similar which will be looked at more detail later. In this research, 'representative' transformed region refers to crack behaviour and interface interactions under rolling–sliding contact, rather than the full thermo-mechanical history of in-service WEL formation.

The transition zone between the transformed region and the underlying pearlitic steel, shown in Figure 16, was also found to be similar when compared to a field sample (from [14]). It should be noted that this comparison is only qualitative, as differences in grain size, crystallographic texture, and deformation history were not assessed in this study. This alignment suggests that the laser process can reliably produce realistic microstructural gradients representative of service-induced damage.

Further evidence of similarity was provided by hardness measurements. Field WELs typically showed microhardness values between 550 and 820 HV [13], [14], as shown in Figure 17. The laser-generated WELs demonstrated a similar range, from 600 to 900 HV, with comparable peak values and spatial distributions. Figure 18 shows a microhardness heatmap before and after twin-disc testing, confirming that both the initial

properties and their evolution under contact conditions closely resemble those found in actual rail environments.

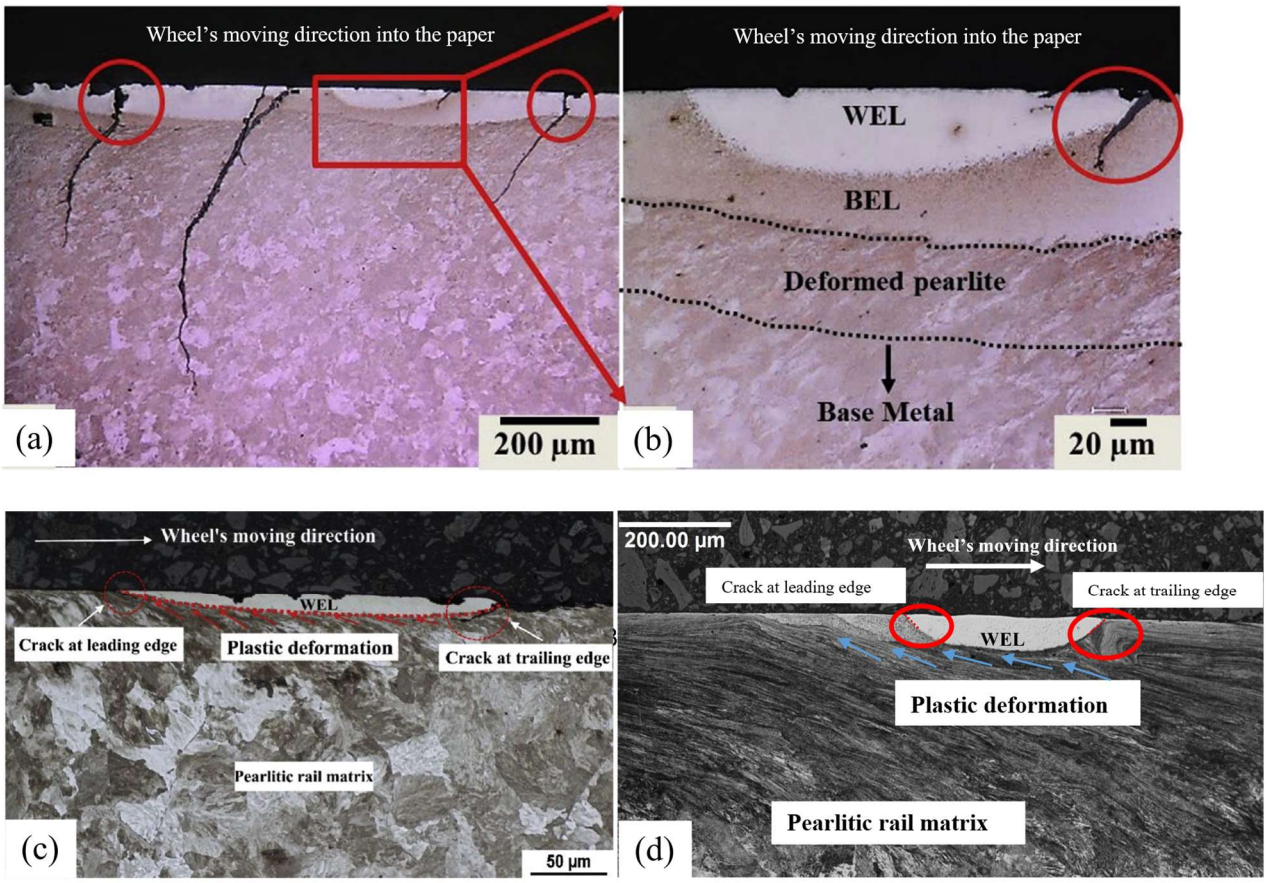

Figure 15 *(a-b) Micrograph of a rail cross-section showing crack initiation and propagation associated with WELs and BELs [19]; (c) Microstructure of cracks in the vicinity of WEL on a head hardened pearlitic rail surface (380HV) [17]; (d) Laser created transformed region in R260 disc - Location A.*

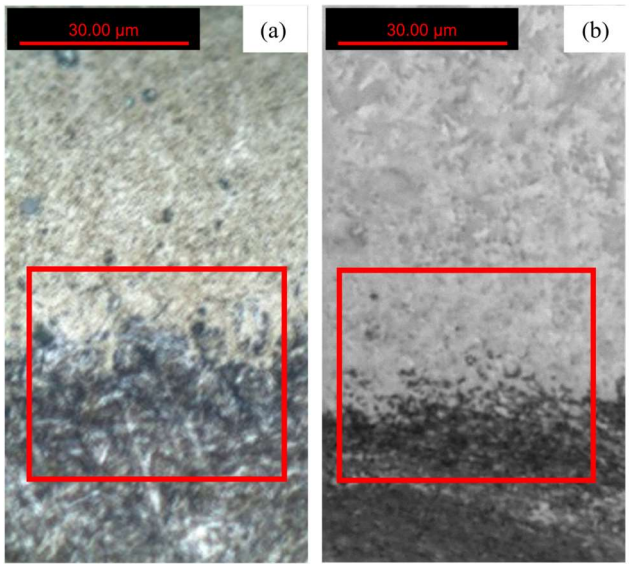

Figure 16 *(a) Transition zone between field WEL and base metal [14]; (b) Transition zone in laser created WEL in R260 - Location A.*

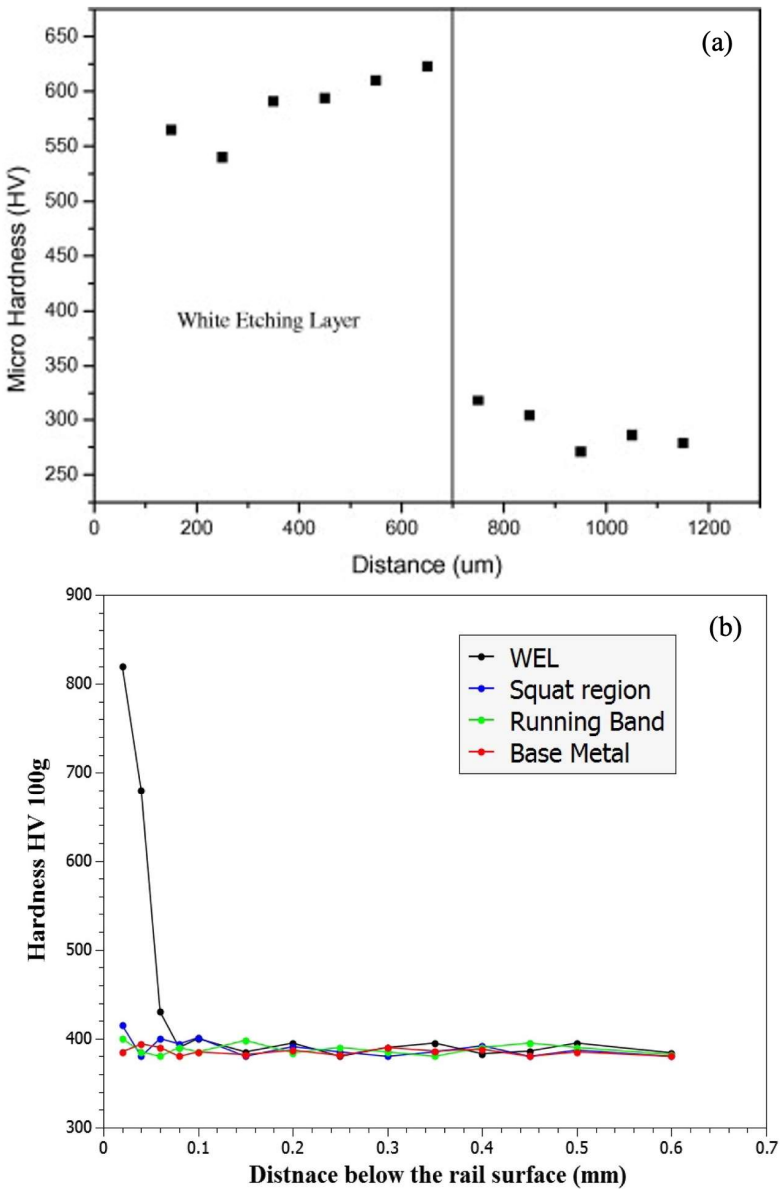

Figure 17 *(a) Microhardness of field WEL [14]; (b) Microhardness profiles measured from track [17].*

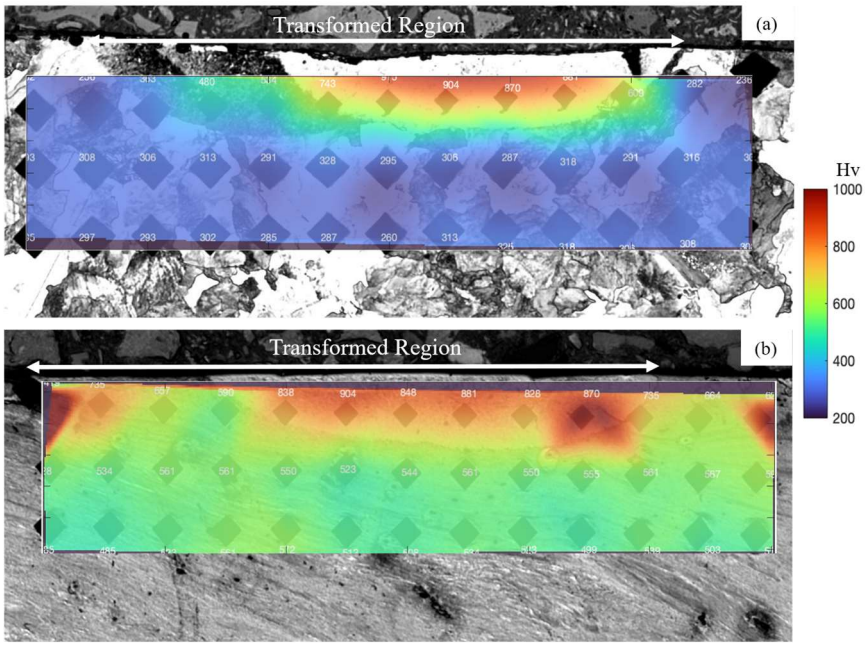

Figure 18 *Microhardness (in Hv) heat map of a transformed region created by laser on R260 grade rail, (a)*

before twin disc test; (b) after twin disc test.

In the twin disc tests three types of crack patterns in the transformed regions were successfully represented, and the crack characteristics observed around the WEL in field samples are very similar to those identified in the R260 specimens after the twin disc tests [14], [20]. Shallow angle leading edge cracks were found in both the field samples, as shown in Figure 19 (a) and (e), and in the post twin-disc test R260 specimens, as shown in Figure 19 (i). As for the internal cracks observed in the field samples, shown in Figure 19 (b), (f), and (g), internal crack angles that were comparable to those found in the R260 specimens, as illustrated in Figure 19 (j). The trailing edge crack in the field sample was observed to propagate along the interface between the WEL and the surrounding bulk material, eventually extending into the WEL at the tip of the extended trailing edge crack.

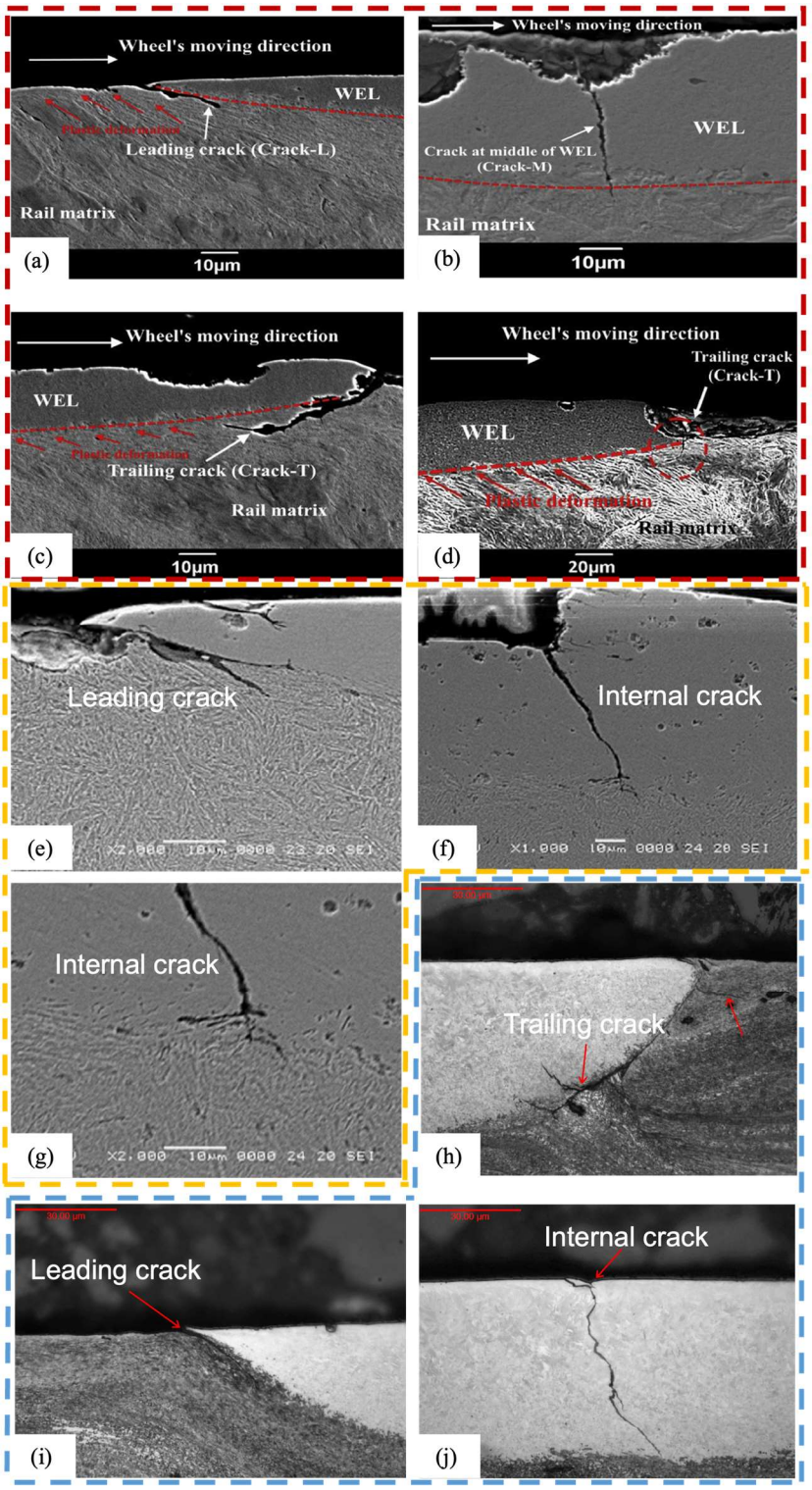

Figure 19 *(a-d) Microscopic features of cracks in WEL obtained by SEM from the field in red box [17]; (e-g) Leading edge and internal WEL cracks in extracted rail from field in yellow box [14]; (h-j) Cracks from laser created WEL in R260 - Location A in blue box.*

4.2. Comparison with previous twin disc tests

The biggest difference between previous research and this work is the material. Freisinger et al. previously used wheel steels ER7 and ER9 for WEL creation and then conducted twin disc tests [10], [11], [12], while this study focused on rail steel R260 grade rail steel. Although both materials can form WELs under thermal or mechanical loads, their mechanical properties and residual stress behaviours differently. These differences may influence crack initiation and growth tendencies, especially under rolling–sliding contact. Since the field

rail defects commonly involve R260 grade rail, the present use of R260 enhances the representativeness of our lab-based simulations in representing actual in-service damages.

Freisinger et al. conducted twin-disc testing on stratified surface layers (SSLs) composed of WELs and brown etching layers (BELs), created on wheel materials ER7 and ER9. Their results consistently showed crack initiation and propagation exclusively at the leading edge of the SSLs. In contrast, no cracking was reported at the trailing edge in any of their specimens after 100,000 cycles. This shows differently from the findings of this study, where cracks were clearly observed at both the leading and trailing edges in laser-generated transformed regions on R260 rail steel after twin-disc testing. The presence of trailing edge cracks in our specimens is consistent with field data, reinforcing the reliability of the laser-based simulation model.

While considering geometry, a possible reason for this difference lies in the geometric characteristics of the WELs. In Freisinger's study, the laser-created WELs were significantly thicker at average of 350 µm, while the thicknesses of transformed regions were only about 60 µm in this research. Also, they had a shallower trailing edge angle compared to this research. These characteristics could reduce the local stress concentration at the trailing edge and suppress crack initiation in that area. The WELs in this work were created much thinner and more sharply angled, may have resulted in a more sudden material transition and higher stress intensities at the trailing edge, which both facilitate crack growth.

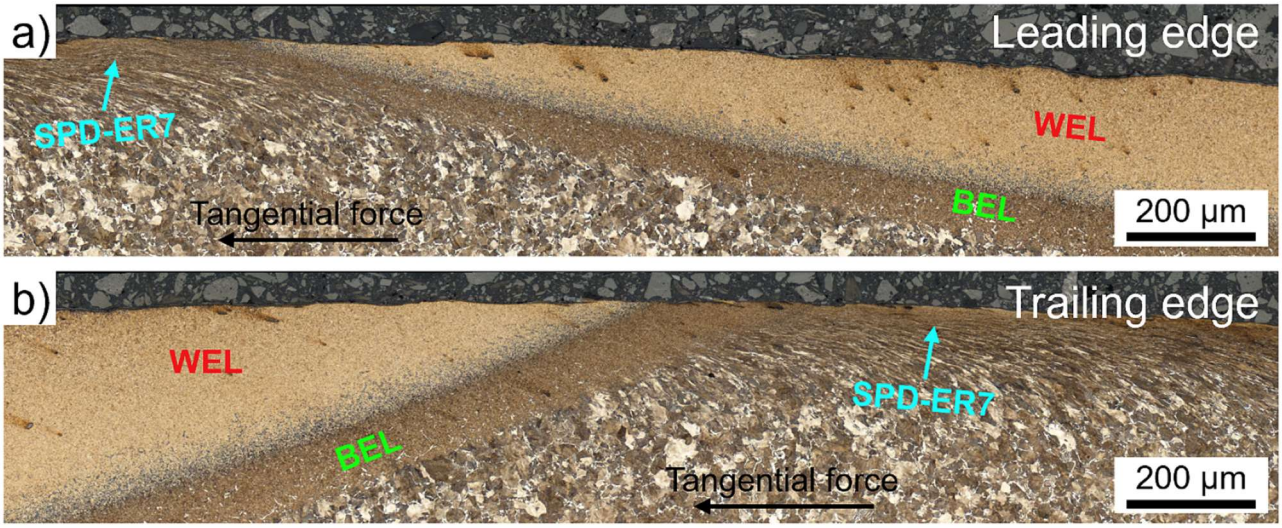

Figure 20 *Sample of WEL & BEL on ER7 wheel steel from previous tests: (a) Leading edge; (b) Trailing edge [12].*

4.3. Comparison to FE Modelling

Previous Finite Element Analysis modelling studies [5, 7] has investigated the stress distribution within the rail material across the region extending from before the WEL to the far side of the contact area. Here the findings are compared with the twin disc test outcomes.

In the present twin-disc tests, greater plastic deformation was observed on the leading side of the specimens, which is consistent with simulation results showing higher stress levels at the leading edge compared to the trailing side [5].

The cracks tended to be longer on the trailing side, where they propagated along the interface between the WEL and the surrounding bulk material. This crack propagation pattern was consistently observed in the twin disc tests. However, the modelling did not fully capture the extent of bulk material deformation, or the stress concentration effect generated at the interface between the WEL and the bulk material, which is clearly present in experimental observations.

The simulated stress profiles revealed the highest stress levels in the region before the WEL and the lowest stress levels after it. A rail-wheel contact model used is shown in Figure 21, where "2a" represents the length of WEL while "b" shows the thickness of WEL. Modelling also showed that contact conditions with a semi

axis ratio (a/b) below values of approximately 4 to 5 resulted in more severe stress concentrations. In contrast, the geometry of the transformed regions produced in this study exhibited larger semi axis ratios, indicating comparatively lower stress severity under specific conditions.

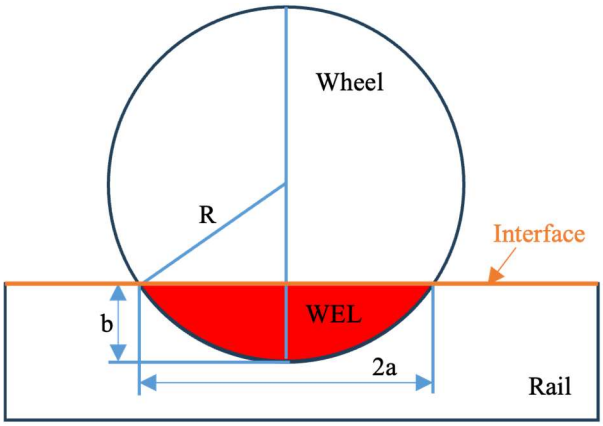

Figure 21 *Schematic diagram of the WEL geometry model [10], [11], [13].*

Further FE analysis reinforced the observation that stresses were higher on the leading side of the WEL as shown in Figure 22 [17]. These modelling results also identified critical threshold values for various crack-related parameters, including crack angle. In the twin disc tests, leading edge cracks exhibited angles of approximately 12°, while trailing edge cracks ranged between 40° and 50°. These angles resulted in similar values for both the J-integral and the stress intensity factors (SIF) [17]. Additional modelling of the wheel and rail interface, incorporating the presence of the WEL demonstrated a clear stress concentration effect at the boundary between the bulk rail material and the WEL [2], which provides a mechanistic explanation for the observed crack propagation paths along this interface.

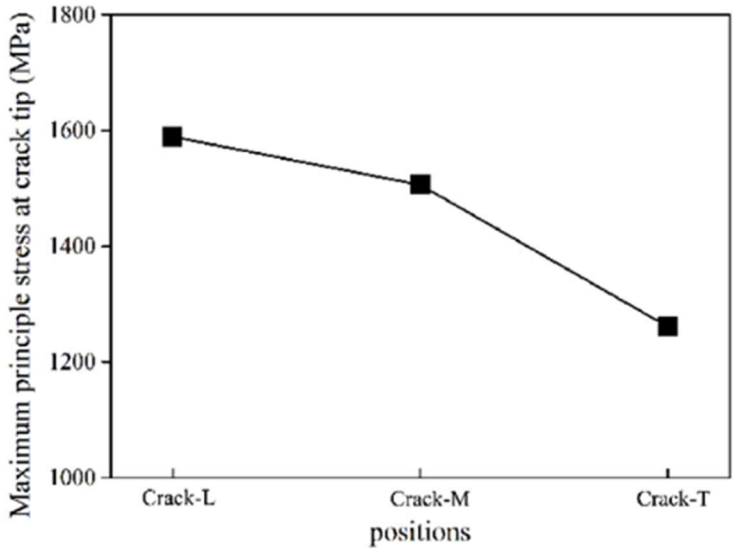

Figure 22 *Stress levels at the leading edge (L), middle of the WEL (M) and trailing edge (T) from FEA [17].*

The elevated stress concentrations on the leading edge observed in the modelling align with the deformation patterns in the bulk material seen in the twin disc specimens. However, the level of deformation at the trailing edge observed in the tests was not reproduced in the simulations, suggesting limitations in the current modelling approach in fully capturing the complex interaction between the WEL and the surrounding bulk material under rolling and sliding contact conditions. The work presented in this paper can help improve such models.

5. Conclusions

This study provides valuable insights into the influence of laser-induced hard transformed regions on the damage behaviour of R260 rail material under rolling-sliding contact conditions. The results highlight the critical role of the WEL in promoting crack initiation and propagation, particularly at the transformed

region/substrate interface and within the transformed region as shown in Figure 23. The presence of localised material deformation, such as twisting and material flow patterns, was found to significantly influence crack initiation and growth, leading to the formation of characteristic Y-shaped junctions. These findings contribute to a deeper understanding of the tribological behaviour of rail materials under contact stress and offer implications for improving the design and maintenance of railway systems. Future work could focus on refining laser treatment parameters and further investigating the long-term behaviour of WELs in service conditions.

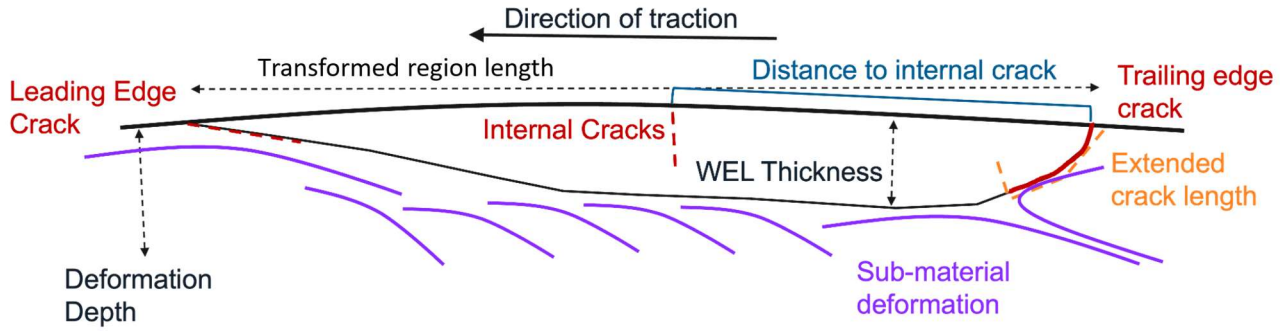

Figure 23 *Characteristic of transformed region deformation under rolling-sliding contact condition.*

In addition, comparison with FEA modelling from previous work offered useful insights into the stress distribution around the WEL and crack predictions, but it did not fully reflect the complex behaviour seen in the experimental results. In particular, the models were limited to replicate the extent of plastic deformation and crack development along the interface between the WEL and bulk material, especially on the trailing edge. This suggests that current modelling approaches may not yet account for important factors such as localised material transformations and interface effects. To more accurately predict damage mechanisms associated with WELs, future modelling efforts should consider incorporating these microstructural and mechanical complexities. Further development to such simulations would be essential for advancing the understanding of rail surface damage and guiding more effective railway industry maintenance strategies.

6. Acknowledgements

The publication was written at the University of Sheffield, UK, and at the Virtual Vehicle Research GmbH in Graz, Austria. The authors would like to acknowledge the financial support within the COMET K2 Competence Centres for Excellent Technologies from the Austrian Federal Ministry for Innovation, Mobility and Infrastructure (BMIMI), Austrian Federal Ministry for Economy, Energy and Tourism (BMWET), the Province of Styria (Dept. 12) and the Styrian Business Promotion Agency (SFG). The Austrian Research Promotion Agency (FFG) has been authorized for the programme management.

The authors would furthermore like to express their thanks to their supporting industrial and scientific project partners, namely Siemens Mobility Austria GmbH, voestalpine Rail Technology GmbH and to the University of Sheffield.

References

[1] J. Seo, S. Kwon, H. Jun, and D. Lee, “Rolling contact fatigue of white etching layer on pearlite steel rail,” *Key Eng Mater*, vol. 417–418, pp. 309–312, 2010, doi: 10.4028/www.scientific.net/KEM.417-418.309.

[2] S. Pal, W. J. T. Daniel, and M. Farjoo, “Early stages of rail squat formation and the role of a white etching layer,” *Int J Fatigue*, vol. 52, pp. 144–156, Jul. 2013, doi: 10.1016/j.ijfatigue.2013.02.016.

[3] R. I. Carroll and J. H. Beynon, “Rolling contact fatigue of white etching layer. Part 2. Numerical results,” *Wear*, vol. 262, no. 9–10, pp. 1267–1273, Apr. 2007, doi: 10.1016/j.wear.2007.01.002.

[4] R. Masoudi Nejad, M. Shariati, and K. Farhangdoost, “Effect of wear on rolling contact fatigue crack growth in rails,” *Tribol Int*, vol. 94, pp. 118–125, Feb. 2016, doi: 10.1016/j.triboint.2015.08.035.

[5] Z. Popovic, L. Lazarevic, M. Micic, and L. Brajovic, “Critical analysis of RCF rail defects classification,” in *Transportation Research Procedia*, Elsevier B.V., 2022, pp. 2550–2561. doi: 10.1016/j.trpro.2022.06.294.

[6] B. Hieu Nguyen, A. Al-Juboori, H. Zhu, Q. Zhu, H. Li, and K. Tieu, “Formation mechanism and evolution of white etching layers on different rail grades,” *Int J Fatigue*, vol. 163, Oct. 2022, doi: 10.1016/j.ijfatigue.2022.107100.
[7] A. Al-Juboori *et al.*, “Squat formation and the occurrence of two distinct classes of white etching layer on the surface of rail steel,” *Int J Fatigue*, vol. 104, pp. 52–60, Nov. 2017, doi: 10.1016/j.ijfatigue.2017.07.005.
[8] P. Merino *et al.*, “An attempt to generate mechanical white etching layer on rail surface on a new rolling contact test bench,” *Wear*, vol. 482–483, Oct. 2021, doi: 10.1016/j.wear.2021.203945.
[9] Y. Yang, A. Aydin, K. Mumtaz, M. Januschewsky, A. Meierhofer, and R. Lewis, “Novel use of laser melting and optical pre-heat to control white etching layer formation on rail steels,” *Tribol Int*, vol. 204, Apr. 2025, doi: 10.1016/j.triboint.2024.110472.
[10] M. Freisinger, K. Pichelbauer, G. Trummer, and K. Six, “Influence of thermal loading parameters and microstructure on the formation of stratified surface layers on railway wheels,” *Proc Inst Mech Eng F J Rail Rapid Transit*, vol. 238, no. 7, pp. 757–764, Aug. 2024, doi: 10.1177/09544097241229121.
[11] M. Freisinger *et al.*, “Comparative study on the influence of initial deformation and temperature of thermally induced white etching layers on rail wheels,” *Tribol Int*, vol. 177, Jan. 2023, doi: 10.1016/j.triboint.2022.107990.
[12] M. Freisinger, B. Jakab, K. Pichelbauer, G. Trummer, K. Six, and P. H. Mayrhofer, “Fatigue crack initiation in the presence of stratified surface layers on rail wheels,” *Int J Fatigue*, vol. 177, Dec. 2023, doi: 10.1016/j.ijfatigue.2023.107958.
[13] Q. Lian, G. Deng, H. Zhu, H. Li, X. Wang, and Z. Liu, “Influence of white etching layer on rolling contact behavior at wheel-rail interface,” *Friction*, vol. 8, no. 6, pp. 1178–1196, Dec. 2020, doi: 10.1007/s40544-020-0388-x.
[14] J. Seo, S. Kwon, H. Jun, and D. Lee, “Numerical stress analysis and rolling contact fatigue of White Etching Layer on rail steel,” *Int J Fatigue*, vol. 33, no. 2, pp. 203–211, Feb. 2011, doi: 10.1016/j.ijfatigue.2010.08.007.
[15] A. D. Bedoya-Zapata *et al.*, “White Etching Layer (WEL) formation in different rail grades after grinding operations in the field,” *Wear*, vol. 502–503, Aug. 2022, doi: 10.1016/j.wear.2022.204371.
[16] A. Al-Juboori *et al.*, “Characterisation of White Etching Layers formed on rails subjected to different traffic conditions,” *Wear*, vol. 436–437, Oct. 2019, doi: 10.1016/j.wear.2019.202998.
[17] Q. Lian *et al.*, “Crack propagation behavior in white etching layer on rail steel surface,” *Eng Fail Anal*, vol. 104, pp. 816–829, Oct. 2019, doi: 10.1016/j.engfailanal.2019.06.067.
[18] J. Wu, R. H. Petrov, M. Naeimi, Z. Li, R. Dollevoet, and J. Sietsma, “Laboratory simulation of martensite formation of white etching layer in rail steel,” *Int J Fatigue*, vol. 91, pp. 11–20, Oct. 2016, doi: 10.1016/j.ijfatigue.2016.05.016.
[19] A. Kumar, G. Agarwal, R. Petrov, S. Goto, J. Sietsma, and M. Herbig, “Microstructural evolution of white and brown etching layers in pearlitic rail steels,” *Acta Mater*, vol. 171, pp. 48–64, Jun. 2019, doi: 10.1016/j.actamat.2019.04.012.
[20] A. Kumar *et al.*, “In situ study on fracture behaviour of white etching layers formed on rails,” *Acta Mater*, vol. 180, pp. 60–72, Nov. 2019, doi: 10.1016/j.actamat.2019.08.060.